Solid State Phenomena
ISSN: 1662-9779, Vols. 32-33, pp 565-570
doi:10.4028/www.scientific.net/SSP.32-33.565

Online: 1993-12-12

HREM AND DLTS OF Σ37(610) AND Σ29(520) [001] TILT GRAIN BOUNDARIES IN Ge BICRYSTALS

N.I. Bochkareva[1], J. Heydenreich[2], S. Ruvimov[1], R. Scholz[2], K. Scheerschmidt[2] and L.M. Sorokin[1]

[1] A.F. Ioffe Physical-Technical Institute, Russian Academy of Science
194 021 St. Petersburg, Russia

[2] Max-Planck-Institut für Mikrostrukturphysik, Weinberg 2
O-4050 Halle/Saale, Germany

ABSTRACT

High resolution electron microscopy (HREM) and deep level transient spectroscopy (DLTS) were applied to study the [001] tilt boundaries with Σ37(610) and Σ29(520) in germanium bicrystals. The various defects like facets, atomic steps, primary and secondary grain boundary dislocations (GBDs) were observed in both types of boundaries. The approximate boundary structures were first revealed by the experimental HREM images taken under different defocus conditions before they were refined by means of a trial-and-error method applying alternatively the image simulation and the molecular static calculation of relaxed structures. The analysis of DLTS spectra indicates the impurity segregation at the boundary and enables us to explain the fluctuations in the potential barrier by the formation of vacancy-type oxygen complexes of a donor-like state at E_C-0.21 eV.

1.INTRODUCTION

The great interest in the atomic grain boundary (GB) structure is supported not only by the practical importance of polycrystalline semiconducting materials but also by the fundamental problem of the relationship between their physical properties and structures [1-3]. For most of the tilt GBs, however, EBIC, DLTS and capacitance measurements seem to demonstrate similar features so that there had no been any evidence of a correlation between the intrinsic GB structure and the electronic properties [2]. Consequently, the latter should be attributed to the point defect agglomerations or/and segregated impurities. Nevertheless, the intrinsic atomic structure influences the point defect agglomerations so that further investigations will be necessary to substantiate these conclusions. During the last years a lot of experimental studies as well as calculations on the structures and energies of symmetrical [001] tilt GBs in silicon and germanium have been carried out [4-11] particulary in connection with a 400 kV HREM [8-10]. More than one stable relaxed structure has also been found for most of the grain boundaries. The present paper describes TEM studies and DLTS measurements of [001] tilt GBs in germanium with Σ = 37 (610) and Σ=29(520).

2. EXPERIMENTAL

The samples were Czochralski-grown on double seeds. As a rule, bicrystals were undoped or doped with Sb at a concentration of $3*10^{-13}cm^{-3}$. The dislocation density in their bulk was about 10^{-4} cm^{-2}. Two precisely oriented seeds (within 0.1 degree) were used. The starting material for the growth experiments was FZ germanium of high purity.

The bicrystals were cut into plates both perpendicular and inclined to the rotation axis [001], then they were mechanically polished on both sides and chemically thinned down to 100 -150 μm. Circular disks of 2 mm in diameter were cut from the plates so that the boundary ran across their centers. Finally, the disks were thinned down to a hole by means of chemical etching or ion milling. JEM-7A and JEM-100C (100 kV) and JEM-4000EX (400 kV) microscopes were used to determine the structure of the boundaries. JEM-100C and JEM-4000EX in the ultra-high resolution mode were equipped with spherical aberrations Cs of 0.7 and 1 mms and with ± 10° and ±15° goniometer stages, respectively. More than nine beams were usually used to yield the atomic structure images. Experimental images taken under different defocus conditions were analysed to get the approximate structure of the boundary core taking into account the geometrical description of the boundary and results of previous studies [4-11]. Thus, several hypothetic structures were revealed to start computer calculations of relaxed structures and the simulation of the HREM images (CERIUS, Molecular Simulation Corp.). A trial-and-error procedure [5] was applied to adjust simulated images to experimental ones.

In accordance with a general geometrical description [6,10] of symmetrical [001] tilt boundaries all of the most important boundary characteristics can be deduced from a couple of integers (k_1,k_2) . For instance, the normal to the boundary plane $n_1=[k_1,k_2,0]$, the interface periodicity $d_p=\alpha[-k_2,k_1,0]$ and the Σ-value is equal to $\alpha(k_1^2+k_2^2)$. The α-value is equal to 0.5 if k_1 and k_2 are odd and 1 otherwise. In both our cases α=1 (see table 1) .

Table 1. Characteristics of the Σ37(610) and Σ29(520)/[001] boundaries

Σ	Θ (°)	GB plane $(k_1,k_2,0)$	CSL period d (nm)	α	Schematic structure
37	18.92	(610)	~ 17	1	ppBpB
29	43.6	(520)	~ 12	1	BBpBp

Following the structural unit models [6-11], the boundary core can be represented by a periodic sequence of a mixture of trigonal-pentagonal units (A or B) or distorted perfect ones (p), or equally by the cores of dislocations with a Burgers vector of 1/2<110> type. In the notation of Rouviere & Bourret [10], A-units correspond to the core of edge dislocations while B-units correspond to 45° ones. Depending on the chirality and the orientation of these units 16 different dislocation cores were revealed [8-11], resulting in a lot of variants possible for the boundary structure. For example, the decomposition of the boundary Burgers vector of <100> type into two A- or B-units leads to a zigzag (Z) or symmetrical (S) boundary model respectively, despite of the ambiguities possible owing to the rearrangement of bonds. To distinguish the two cases which both can be labelled $S_{2,1}$ or $Z_{2,1}$, the most probable unit configurations (see text below) are given in the table.

The samples of 3×3×9 mm^3 in size were prepared for electrical measurements so that the boundary passes through the centre of the 3×3 mm^2 face parallel to 3×9 mm^2 face. Both types of samples were studied, i.e. those protected by wet-resistant lacquer to avoid surface aging (I-type) as well as the unprotected (II-type) ones. Capacitance measurements and DLTS scans were performed over the temperature range of 70-300 K using a RF admittance bridge.

3. RESULTS AND DISCUSSION

3.1 Σ37(610)/[001] BOUNDARY.

Different bicrystals studied as well as their different parts show various degrees of boundary plane faceting (see figures 1, 2). Figure 1 shows micrographs typical of the weakly faceted boundary at different magnifications and differently inclined to the transmitted beam. Both primary and secondary dislocations are revealed as rows of lines parallel to the tilt axis [001].

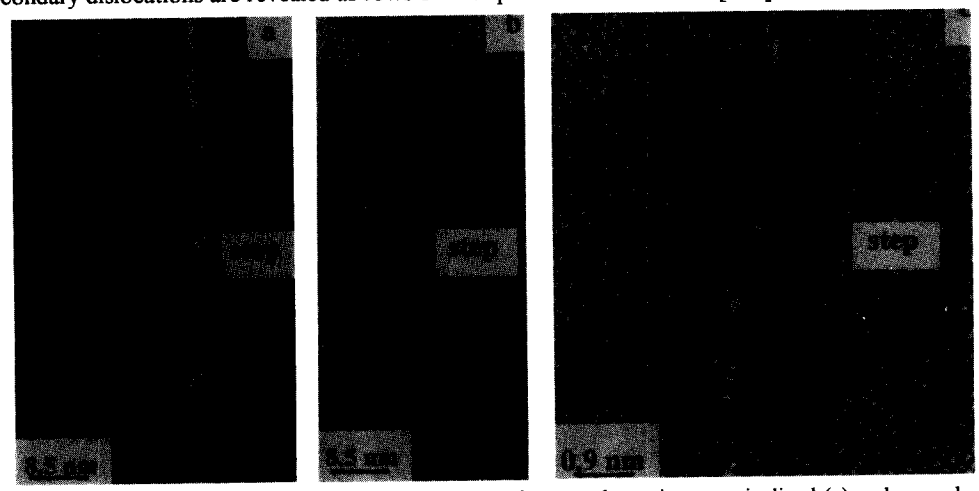

Figure 1. Weakly faceted Σ37(610)/[001] boundary. a,b- many beam images - inclined (a) and normal (b) to [001], c- 400kV-HREM image.

A faint oscillatory contrast on the inclined boundary plane is shown in figure 1a. The secondary dislocations in the image are revealed as a brighter contrast at the place of two primary lines. The periods of the primary and secondary dislocation spacings are 1.7 nm and 15 - 25 nm , respectively. Figure 1b demonstrates the image of the boundary in the edge-on position as a sequence of black dots spacing of which are equal to those of the primary period. The secondary dislocations are localized in primary dots resulting in the reduction of their sizes. They are marked by arrows because the reduction of their sizes is not so obvious. A weak dark contrast around these dots is due to the strain fields of secondary dislocations. The deviation of primary period from 1.7 to 1.45 nm is easily observed in HREM images with a change in the structure every 10-15 primary periods (17-25 nm). Such variations of the primary period could be described as local irregularities of the arrangement of structural units. While the basic period is equal to d = a/2 [610] the deviating one is equal to d' = a/2 [510], i.e. it corresponds to the Σ= 13(510)/[001] boundary. All primary dots are slightly elongated in a trace direction indicating the dissociation of primary dislocations, which was observed before by the splitting of each primary line [12].

The structure of the Σ37(610)/[001] boundary can be represented by various combinations of (2A,3p) or (2B,3p) units, or their mixture. The analysis of images of a weakly faceted boundary shows that the (B,p,B,p,p) sequence (S-type model) seems to be a better model than the Z-type one as the first approach to the boundary structure . This model is equivalent to the dissociation of the primary period into two 45°- dislocations. Further trying to better fit the simulated images to experimental ones leads us to more complicated structures as e.g. IH^{+-}or IV^{+-}, which were earlier suggested in [8-11] to describe the similar boundaries (Σ25(710) and Σ41 (910)). However, they also

cannot be considered sufficient enough and require further refinements. Moreover, core contrast is not so distinct in most of the cases, pherhaps, owing to a small twist component of grain misorientation reducing the image resolution. Besides, their images slightly differ for various primary periods. The impurity segregation is likely to influence the core images, too. The presence of impurities at the boundary results in the appearence of a wall of higher thickness containing the boundary, when the samples were finally thinned by ion milling, or grooves during chemical etching.

One can see also steps in the images of figures 1-3. Most of them are associated with brighter contrast of neighbouring primary lines (figure 1a). It is easy to detect the presence of lattice dislocations. HREM images (figures 1c,2c) confirm these conclusions.

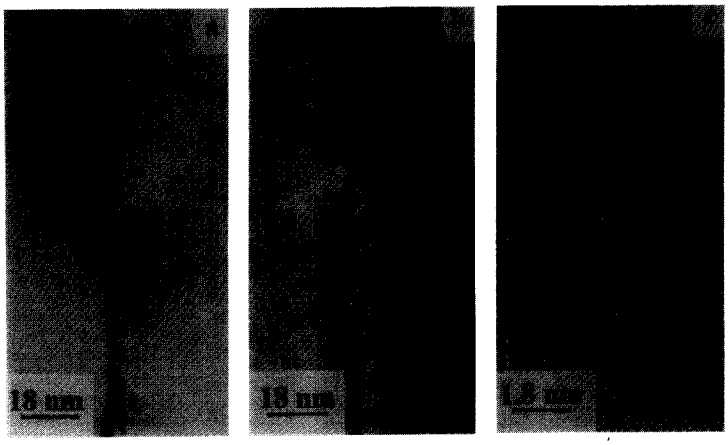

Figure 2. Strongly faceted Σ37(610)/[001] boundary at different inclinations to the transmitted beam: a,b-many beam images inclined (a) and normal (b) to [001], c- 400 kV-HREM image

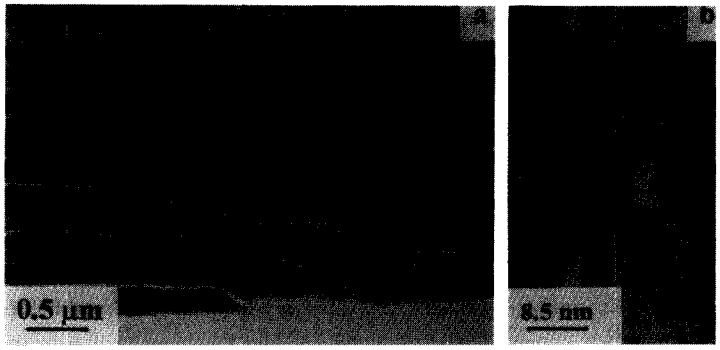

Figure 3. Plan-view image of a faceted Σ 37(610)/[001] boundary (a) and a fragment of a small twist facet normal to [001] (b).

It was established that the surface of a strongly faceted boundary is corrugated and consists of a set of planar regions 20 to 500 nm long, both symmetric and asymmetric. The latter are deflected from the symmetric position by an angle up to 20 degrees (figure 2b). Some of the boundaries consist of alternating asymmetric parts close to the $(100)_1$ //$(310)_2$ orientation of the first grain related to the second one and vice versa. According to the coincidence site lattice (CSL) for $\Sigma = 37$ these planes have a high density of atoms. In the plan-view image presented in figure 3a a strongly faceted boundary is shown as a terrace-like surface, which consists of planar regions separated by

steps. The latter are fragments of both asymmetric tilt boundaries and twist ones, one of which is shown in figure 3b.

3.3 Σ29(520)/[001] BOUNDARY

Contrary to the Σ37(610) GB with $k_1 \geq 3k_2$ the Σ29(520) boundary is characterized by $k_1 \leq 3k_2$ representing a different kind of GBs. Therefore one can expect an essential difference in their structures. Figure 4 shows typical boundary images under different diffraction conditions, magnifications and for different spacing positions. While similar defects like facets, atomic steps, primary and secondary GBDs are observed in the images the atomic structure of the boundary essentially differs from Σ37(610). Figure 4b demonstrates a lot of contrast variations of primary dots. Secondary dislocations and boundary steps divide the bands of different contrast producing the black-white contrast around them. A geometrical analysis predicts a (3A,2p) or a (3B,2p) sequence of structure units for the Σ29(520) boundary core. Our results show that Z-models (for instance, BBpBp, table 1) are more probable, which is in contrast to the results of Rouviere & Bourret [10] where the S-model was found to be more reliable for similar Σ13(320) GB.

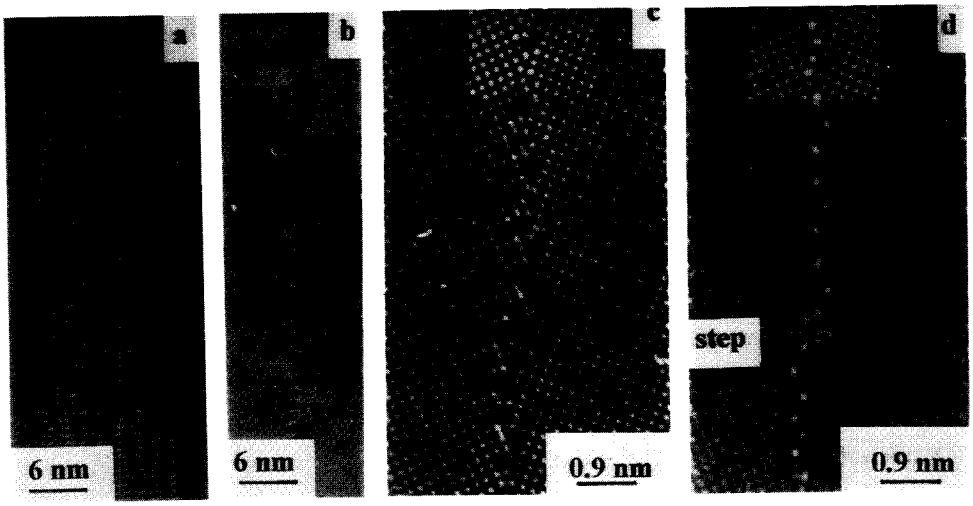

Figure 4. Σ29(520) boundary : a,b- many beam images both inclined (a) and normal (b) to [001], 400 kV-HREM images for different defocus values with inserted simulations (c:-70 nm, white atoms ,d: -40 nm, black atoms).

3.2 DLTS.

DLTS spectra of a Σ37 (610) boundary also evidence the impurity segregation at the boundary. Figure 4 presents a typical DLTS spectra. A detailed analysis of capacitance, conductance and DLTS data will be given elsewhere [13]. Here, we consider some conclusions and their correlations with structural observations. DLTS data show that the current across the boundary at low voltage happens via the recombination of holes, thermally generated in the quasi-neutral space charge regions, with electrons in the boundary states. The accumulation of holes at the boundary following a voltage pulse gives rise to DLTS peaks with activation energies of 0.74 and 0.39 eV . The DLTS peak at 0.21 eV is related to the clusters of oxygen-vacancy complexes with donor-like states at E_C-0.21 eV.

The excess conductance and capacitance of a bicrystal result from fluctuations of the potential barrier owing to the compensation of dislocation-related acceptor states by donor states of the oxygen complexes. In the previous studies [14] of Si bicrystals the charge sites within the grain boundary have been related to the spatial distributions of secondary dislocations. The characteristic distances of secondary GBDs in our cases are in good agreement with the average charge spacings (~25 nm) deduced from the capacitance values. Therefore the electrical activity of the GB may be related to the secondary GBDs rather than to the intrinsic boundary structure.

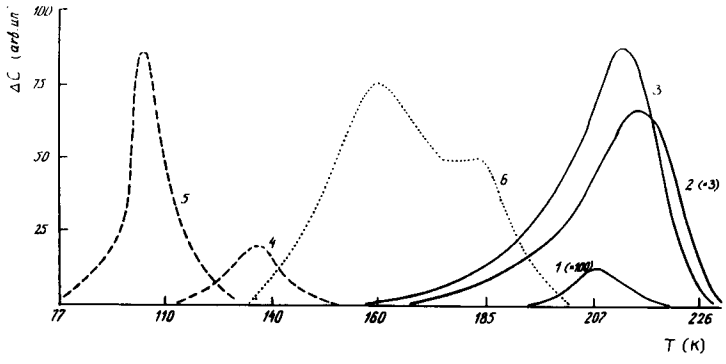

Figure 5. DLTS spectra of Σ 37(610) GB (samples I: full curves; samples II: broken ones) and reference Ge crystal (dotted curves) measured at $U+U_p \rightarrow U$ switch (V): $0.05 \rightarrow 0$ (1), $0.6 \rightarrow 0$ (2), $1 \rightarrow 0$ (3-5), $0 \rightarrow 2$ (6). f=150 kHz Curves 4,5 correspond to aging samples.

The data analysis allows us to suggest a model of the boundary potential relief. Dislocations in Ge are known to be associated with shallow acceptor-like states [15]. The Fermi level position at the boundary is close to the top of the valence band if the impurity concentration is low. Donors of the oxygen complexes can "compensate" these acceptor-like states and pin the Fermi level at about $E_c - E_g/2 - 0.21$, or, at $E_c - 0.21$ eV if the oxygen concentration is high enough. This is the reason for the "valleys" in the potential barrier in the bulk and on the surface, and for the boundary broadening, which produces the excess current across the boundary and anomalous DTLS spectra.
This model can also explain the DC and HF steady-state and the transient behaviour of GBs in other materials (Si, GaAs, ZnO).

REFERENCES

1). Seager C.H., Pike G.E.& Ginley D.S. Phys.Rev.Lett., 1979, **43**, 532
2). Broniatowski A. & Bourgoin J.C. Phys.Rev.Lett., 1982, **48**, 424
3). Bochkareva N.I., Lelikov Yu.S., Lubalin M.D. & Schreter Yu.G., Fiz.Techn.Poluprov., 1986, **20**, 1396,
4). D'Anterrochers C., Bourret A., Phil.Mag., 1984, **A49**, 783
5). Bacmann J.J., Pappon A.M., Petit M. & Silvestre G., Phil.Mag., 1985, **A51**, 697
6). Kohayma M., Phys.St.Sol., 1987, **b141**, 71
7). Bourret A., Rouviere J.L. & Penisson J.M., Acta Cryst., 1988, **A44**, 838
8). Bourret A., Rouviere J.L., in Polycristalline Semiconductors (Ed.J.H.Werner, H.J.Möller, H.P.Strunk), Springer -Verlag, Berlin, 1989, p.8
9). Rouviere J.L., Bourret A., Ibid., p.19
10). Rouviere J.L., Bourret A., J.Physique Coll., 1990, **51**, C1, 329
11). Levi A.A., Smith D.A., Wetzel J.T., J.Appl.Phys., 1991, **69**, 2048
12). Bochkareva N.I., Ruvimov S.S., Scholz R., Scheerschmidt K. & Sorokin L.M., Inst.Phys.Conf.Ser., 1993, to be published
13). Bochkareva N.I., Mosina G.N., Ruvimov S.S., Scholz R., Sem.Sci.&Techn., 1993, to be published
14). Werner J. & Strunk H., J. Physique Coll., 1982, **89**, C1
15). Bochkareva N.I., Sov.Phys.Sem.,1991, **25**, 323